Using Single-Doppler Data to Obtain a Mesoscale Environmental Field

ALAIN CAYA

Department of Atmospheric and Oceanic Sciences, McGill University, Montreal, Quebec, Canada

STÉPHANE LAROCHE

Meteorological Research Branch, Atmospheric Environment Service, Dorval, and Cooperative Center for Research in Mesometeorology, Montreal, Quebec, Canada

ISZTAR ZAWADZKI

Department of Atmospheric and Oceanic Sciences, McGill University, and Cooperative Center for Research in Mesometeorology, Montreal, Quebec, Canada

THIBAUT MONTMERLE

Department of Atmospheric and Oceanic Sciences, McGill University, Montreal, Quebec, Canada

(Manuscript received 2 November 2000, in final form 11 July 2001)

ABSTRACT

A 3D wind analysis based on single-Doppler data is proposed using mass conservation and assuming a linear horizontal wind field, which is constant in a moving reference frame. Data over an assimilation period that includes several volume scans are employed, allowing the retrieval of the full linear wind field, including vorticity. The method proposed here can be considered an extension of the volume velocity processing (VVP) procedure. The robustness of the method is examined in detail and a criterion on the condition number is obtained. The method is tested in the context of synthetic data, which respect the simplified model assumptions. Simulated data from a high-resolution numerical weather prediction model are used to assess the impact of errors in the simplified model. The results indicate that 1) the analysis improves as the assimilation period is lengthened up to 1 h, 2) the best results are obtained when the radar is surrounded by precipitation and is in the middle of the analysis domain, and 3) vorticity is the most sensitive parameter. The addition of a vertical smoothing constraint is shown to be beneficial for the minimization and improves the results.

1. Introduction

The J. S. Marshall Radar Observatory of McGill University operates a bistatic radar network that comprises one S-band Doppler radar and two low-gain nonscanning receivers (Kilambi et al. 1997). Protat and Zawadzki (1999) have developed a method for retrieving the 3D wind field from the bistatic network observations. The evolution of their 3D wind field provides perturbations of pressure and temperature from the momentum equations (Protat et al. 2001). However, for purposes of model initialization, the flow outside the bistatic region or in precipitation-free areas needs to be estimated. Presently, most operational forecast models do not provide a background atmospheric state that is adequate at the convective scale, or necessarily consistent with that retrieved from observations. In the present study, an alternative to this problem is investigated.

Lin et al. (1993) propose a technique to fill data voids in the environment of a storm using a nearby sounding. The continuity of the flow between the environment and the perturbed area is assured by a relaxation method. This technique works well only if the flow surrounding the storm is uniform. When the storm is not isolated but is embedded in a more complex structure, the mesoscale circulation cannot be reduced to a simple uniform flow. In this case, additional soundings near the storm, which are usually not available, would be necessary to retrieve the full wind field.

The Multiple Analytical Doppler (MANDOP; Scialom and Lemaître 1990; Lemaître and Scialom 1992) method uses analytical formulas of the wind field to generate a smoothed field that fits the dataset. Montmerle and Lemaître (1998) use this technique to concurrently assimilate radar and radiosonde data to ini-

Corresponding author address: Alain Caya, Dept. of Atmospheric and Oceanic Sciences, McGill University, 805 Sherbrooke St. West, Montreal, QC H3A 2K6, Canada.
E-mail: caya@zephyr.meteo.mcgill.ca

TABLE 1. Statistics of the difference between control and retrieved radial and tangential components at time $t = 55$ min in areas where reflectivity is less than 15 dBZ for different assimilation periods. A 0-min assimilation period corresponds to VVP.

Assimilation period	Bias (m s^{-1})		Standard deviation (m s^{-1})		Correlation		Condition number
	V_r	V_t	V_r	V_t	V_r	V_t	
0	0.88	0.57	2.59	3.75	0.96	0.86	16
10	0.73	1.69	2.63	4.04	0.96	0.85	19
20	0.73	1.44	2.57	3.77	0.96	0.87	19
30	0.73	1.24	2.46	3.48	0.96	0.88	20
40	0.76	1.02	2.43	3.28	0.96	0.90	22
50	0.83	0.77	2.48	3.17	0.96	0.90	25
60	0.92	0.62	2.55	3.14	0.96	0.90	28

tialize a nonhydrostatic atmospheric model. This method has been successfully applied to data collected during the 22 February case of the Tropical Ocean Global Atmosphere Coupled Ocean–Atmosphere Response Experiment (TOGA COARE; Webster and Lukas 1992), which extensively probed both the storm and its environment.

In a more operational setting, Sun and Crook (2001) attempt to take into account the mesoscale circulation around sampled storms. They argue that using single-Doppler methods to obtain a linear wind is currently more reliable than using a short-range mesoscale model forecast. Such an analysis can be obtained from volume velocity processing (VVP; Waldteufel and Corbin 1979) or by Velocity–Azimuth Display (VAD; Lhermitte and Atlas 1961; Browning and Wexler 1968), which is a particular type of VVP.

Koscielny et al. (1982) suggest that VVP is applicable even for small areas of data while Matejka and Srivastava (1991) find that this is not possible with VAD. On the other hand, Srivastava et al. (1986) argue that VAD is a more robust technique than VVP because of the choice of orthogonal basis functions in VAD. Boccippio (1995, hereafter referred as B95) reconcile these viewpoints by showing that both VAD and VVP are constrained to almost full azimuthal coverage (gaps of greater than 30° should not be allowed without careful inspection of the analysis) and that VVP can be made as robust as VAD. This is because the basis functions in VAD are orthogonal only in the limit of full azimuthal coverage. Caya and Zawadzki (1992) argue that VAD adjustment to Doppler data leads to a correct linear wind only if the actual wind field respects the hypothesis of linearity. In other words, even a perfect VAD fit to radial velocity data does not guarantee that the derived tangential velocity represents the best linear fit to reality.

Vorticity can be evaluated with single-Doppler radar data only if additional assumptions are made about the wind field (Waldteufel and Corbin 1979; Passarelli 1983). The synthetic dual-Doppler analysis technique has been used to circumvent the problem (Pearce et al. 1969; Klimowski and Marwitz 1992; Bluestein et al. 1994), and is based on the frozen turbulence hypothesis. However, this method is likely to fail for rapidly evolving storms or for slowly moving systems. The frozen turbulence hypothesis is a better assumption if long-lived features are observed.

In this paper, we present a method to specify the 3D environmental flow for the analysis of mesoscale characteristics surrounding precipitation areas. The environmental wind field is assumed linear and constant on a moving reference frame and verifies exactly the anelastic continuity equation. In section 2, the method is described in detail. We compare the characteristics of the method with traditional VVP in section 3. A numerical simulation of convective events is then used to generate synthetic data to further test the performance of the method in section 4. Finally, section 5 summarizes the results.

2. Description of the method

a. Expression of the linear wind

A horizontal linear wind model can be expressed as follows:

$$u(x,y,z) = u_o(z) + u_x(z)(x - x_o) + u_y(z)(y - y_o),$$
$$v(x,y,z) = v_o(z) + v_x(z)(x - x_o) + v_y(z)(y - y_o). \quad (2.1)$$

Subscripts x and y indicate spatial derivatives and (x_o, y_o) is the position of the radar site. With this time-independent model, it is impossible to retrieve the vorticity $(v_x - u_y)$ from a single scanning radar (Doviak and Zrnić 1993). To circumvent this problem, the wind field defined by Eq. (2.1) is allowed to move at a constant translation speed during a given assimilation period. The proposed method is thus an extension of VVP. To keep track of the vorticity, we express the linear wind field in terms of divergence D, vorticity ζ, stretching deformation τ, and shearing deformation χ. The horizontal wind field can thus be expressed as

TABLE 2. Statistics of the difference between control and retrieved radial and tangential components at time $t = 55$ min in areas where reflectivity is less than 15 dBZ for different locations of the radar.

Radar position	Bias (m s^{-1})		Standard deviation (m s^{-1})		Correlation		Condition number
	V_r	V_t	V_r	V_t	V_r	V_t	
North	1.82	1.05	2.68	3.75	0.89	0.66	71
East	0.86	2.80	1.92	5.16	0.89	0.65	93
South	0.15	0.84	2.53	3.48	0.97	0.87	60
West	1.43	−0.21	2.61	3.86	0.93	0.83	31
Center	0.92	0.62	2.55	3.14	0.96	0.90	28

$$u(x, y, z, t) = u_o(z) + \left[\frac{D(z) - \tau(z)}{2}\right][x - u'(t - t_o)] + \left[\frac{\chi(z) - \zeta(z)}{2}\right][y - v'(t - t_o)],$$

$$v(x, y, z, t) = v_o(z) + \left[\frac{\chi(z) + \zeta(z)}{2}\right][x - u'(t - t_o)] + \left[\frac{D(z) + \tau(z)}{2}\right][y - v'(t - t_o)], \quad (2.2)$$

where

$$D(z) = u_x(z) + v_y(z), \qquad \tau(z) = v_y(z) - u_x(z),$$

$$\chi(z) = v_x(z) + u_y(z), \qquad \zeta(z) = v_x(z) - u_y(z), \quad (2.3)$$

and (u', v') are the moving frame velocity components, t is the time in the assimilation period, and t_o is the initial time. The radar is located at the origin of the system coordinates $[(x_o, y_o) = (0, 0)]$ to remove the ambiguity between the mean wind (u_o, v_o) and the vorticity ζ (Doviak and Zrnić 1993; Caya and Zawadzki 1992).

b. Scanning radar measurements

When the horizontal wind field is given by (2.2), the scanning radar measures radial velocities according to

$$\mathbf{V}_r(x, y, z, t) = X\boldsymbol{\theta}_p = \begin{bmatrix} \sin(\beta)\cos(\phi) \\ \cos(\beta)\cos(\phi) \\ \frac{r}{2}\cos(\phi) \\ \frac{r}{2}\sin(2\beta)\cos(\phi) \\ \frac{r}{2}\cos(2\beta)\cos(\phi) \\ (t - t_o)\sin(\beta)\cos(\phi) \\ (t - t_o)\cos(\beta)\cos(\phi) \\ \sin(\phi) \end{bmatrix}^{\mathrm{T}} \begin{bmatrix} u_o(z) \\ v_o(z) \\ D(z) \\ \chi(z) \\ \tau(z) \\ -\left(\frac{(D(z) - \tau(z))}{2}u' + \frac{(\chi(z) - \zeta(z))}{2}v'\right) \\ -\left(\frac{(\chi(z) + \zeta(z))}{2}u' + \frac{(D(z) + \tau(z))}{2}v'\right) \\ w(z) + V_T \end{bmatrix}, \quad (2.4)$$

where β is the azimuth measured clockwise from the north, ϕ is the elevation angle, r is the horizontal distance from the radar, and X is the operator acting on the vector θ_p of "p" parameters to be estimated. The matrix representation here is the same as that used by Doviak and Zrnić (1993) for the linear wind. Here the mass-weighted precipitation fall speed V_T is theoretically calculated from the reflectivity field assuming a Marshall–Palmer (1948) drop-size distribution and there is no attempt to retrieve it. By scanning the system as it moves with respect to the radar, the complete circulation is revealed by the effect of different viewing angles of the system.

The vertical wind $w(z)$ introduced in (2.4) is not constrained by a linear form. However, since w is not well measured by operational scanning radars because of low elevation angles, the anelastic continuity equation

$$D(z) = \frac{w(z)}{H} - w_z(z), \quad (2.5)$$

is employed as an additional constraint. Here H is the scale height (set to 10 km). The vertical motion and its

derivative (w_z) are evaluated by vertical discretization on a staggered grid. Expression (2.5) is used as a strong constraint and the divergence is eliminated from the control variables. Thus, the fitted parameters (control variables) are the mean winds $u_o(z)$ and $v_o(z)$, vertical motion $w(z)$, stretching $\tau(z)$, shearing $\chi(z)$, vorticity $\zeta(z)$, and the moving frame (u', v'). In addition, zero vertical motion is imposed at the ground and one grid point above the highest echo, as in Protat and Zawadzki (1999).

c. The cost function

The wind field is obtained by solving the following weighted least squares estimator with the wind model (2.2) as a strong constraint:

$$J = J_o + J_s, \tag{2.6}$$

where

$$J_o = (\mathbf{V}_r - \mathbf{V}_r')^{\mathrm{T}}\mathbf{C}_r^{-1}(\mathbf{V}_r - \mathbf{V}_r'), \tag{2.7}$$

$$J_s = \gamma_h\left(\frac{\partial^2 u}{\partial z^2}\Delta x^2\right)^2 + \gamma_h\left(\frac{\partial^2 v}{\partial z^2}\Delta x^2\right)^2 + \gamma_v\left(\frac{\partial^2 w}{\partial z^2}\Delta x^2\right)^2, \tag{2.8}$$

where $\mathbf{V}_r'$ is the observed radial velocity and $\mathbf{C}_r$ is the observational-error covariance matrix ($\mathbf{C}_r = \mathrm{E}[(\mathbf{V}_r^t - \mathbf{V}_r')(\mathbf{V}_r^t - \mathbf{V}_r')^{\mathrm{T}}]$ where $\mathbf{V}_r^t$ is the truth). A vertical smoothness constraint J_s is included in the cost function (Wahba and Wendelberger 1980). Otherwise, the vertical coherence must come from the data alone. The γ constants are weights controlling the strength of the vertical smoothness constraint. The corresponding truncation length scale is roughly $l \approx \gamma^{1/4}/\Delta x$, ($\Delta x$ is the horizontal resolution), which depends on the observational-error statistic ($\mathbf{C}_r$). The vertical smoothing is applied here as a weak constraint, as opposed to the VVP model used in B95 where it is applied as a strong constraint. Indeed, the wind in the VVP model of B95 has a linear dependency on height, which is equivalent to the limit $\gamma \to \infty$ in (2.8).

The weights associated with the smoothing constraint are difficult to estimate and objective methods to determine the weights are still a topic of active research. Studies suggest that optimal weights are probably case dependant and can be evaluated by the method of cross-validation suggested by Wahba and Wendelberger (1980).

Error covariances in space are neglected, although the residuals of a linear wind fit through a nonlinear flow are not random but are correlated in space and time. Nevertheless, $\mathbf{C}_r$ is simply taken to be a diagonal matrix.

The first-order derivatives of J with respect to the parameters to be fitted yield the so-called normal equations. Since the wind model used is actually nonlinear in the parameters, the functional J is not quadratic and the normal equations are nonlinear. Consequently, methods for solving sets of linear equations are not applicable here. For the minimization of J, we thus use the quasi-Newton algorithm of Gilbert and Lemaréchal (1989).

First attempts to minimize J involving all fitted parameters failed. We found that the moving frame and the vorticity could not be obtained simultaneously when starting the minimization from a null first guess, which is too far from the final solution. To reach the minimum efficiently, we have adopted the following three-step procedure. First, a minimization is performed setting the vorticity to zero and holding the moving-frame velocity components (u', v') constant. All other fitted parameters are allowed to vary during this process. Then a second minimization stage is initiated at the final point of the first, in which all control variables are allowed to vary except the vorticity. Finally, a third minimization is conducted in which all fitted parameters are allowed to vary, including vorticity.

d. The moving frame

A first guess for the moving frame (u', v') may be estimated by the translation of the reflectivity pattern (Gal-Chen 1982) that minimizes the cost function

$$J_{mv}(u', v') = \sum_{xyzt}\left[\psi\left(x + \frac{u'\Delta t}{2}, y + \frac{v'\Delta t}{2}, z, t_{i+1}\right) - \psi\left(x - \frac{u'\Delta t}{2}, y - \frac{v'\Delta t}{2}, z, t_i\right)\right]^2, \tag{2.9}$$

where ψ is the reflectivity and Δt is the length of the volume interval (typically 5 min). Use of the moving frame estimated from the translation of the reflectivity pattern is examined in section 4c.

Alternatively, translation of the radial velocity pattern can also be considered if the scanning radar is far enough from the analysis domain. This is because radial velocity conservation is a reasonable assumption if azimuth angles change little as the observed system moves. Indeed, the total variation of radial velocity for negligible elevation angle ϕ, is

$$\frac{dV_r}{dt} = \frac{du}{dt}\sin(\beta) + \frac{dv}{dt}\cos(\beta) + [u\cos(\beta) - v\sin(\beta)]\frac{d\beta}{dt}. \tag{2.10}$$

Assuming that the flow does not change in a reference frame,

$$\frac{dV_r}{dt} = V_t\frac{d\beta}{dt}, \tag{2.11}$$

where V_t is the tangential velocity. The translation of the radial velocity pattern technique is not a good can-

didate to estimate the moving-frame velocity since the method we propose requires large differences between viewing angles β, and because the tangential velocity is not negligible in general. Nevertheless, Gal-Chen (1982) demonstrated that it is possible to estimate the moving-frame velocity from the radial velocity field and the frozen turbulence hypothesis. However, Shapiro et al. (1995) showed that there are potentially multiple solutions to the problem. For these reasons, only the translation of the reflectivity pattern is considered in this study to estimate the moving frame.

e. Presence of multiple colinearities

The coefficients of $\sin(\beta)$ and $\cos(\beta)$ in (2.4) are functions of several fitted parameters. This may diminish the robustness of the method, as shown in B95. Indeed, if we consider a 2D model (only one vertical level), and even if the VVP parameters [all the parameters in (2.4) except the vorticity and the moving frame velocities] are well constrained by the data at $t = t_o$, the same radial velocity field at $t \neq t_o$ can be obtained with different sets of ζ and (u', v') according to the following formulas:

$$\frac{(D - \tau)}{2}u' + \frac{(\chi - \zeta)}{2}v' = k_1, \tag{2.12}$$

$$\frac{(\chi + \zeta)}{2}u' + \frac{(D + \tau)}{2}v' = k_2, \tag{2.13}$$

where k_1 and k_2 are the coefficients of $(t - t_o)\sin(\beta)\cos(\phi)$ and $(t - t_o)\cos(\beta)\cos(\phi)$ in (2.4), respectively. After some algebraic manipulations, we find

$$u' = \frac{k_1 v_y - k_2 u_y}{u_x v_y - v_x u_y}, \tag{2.14}$$

$$v' = \frac{k_2 u_x - k_1 v_x}{u_x v_y - v_x u_y}. \tag{2.15}$$

When isolines of u and v (straight lines for a linear wind field) are parallel ($u_x v_y = v_x u_y$), there is no solution for the moving frame and the vorticity. Considering now a model applied to two vertical levels and setting the coefficients of $\sin(\beta)$ and $\cos(\beta)$ at each level to be the same, one has four equations with four unknowns (ζ_1, ζ_2, u', and v'). In this case, the equations are nonlinear and the algebra leads to a one-variable third-order polynomial equation, with up to three possible solutions. Hence, there should be at least three levels in the model for a unique solution. In our experiments with a three-level model, the minimization by the algorithm often ends in a secondary minimum. For this reason, at least four levels in the model should be used. We note that the method would fail if isolines of u and v are parallel at all levels, and the storm motion is along these lines. Although this particular configuration seems quite improbable, a climatology of system structure should answer this question more appropriately. Nevertheless, the method can give good results for the other parameters [u_o, v_o, $w(z)$, $\tau(z)$, and $\chi(z)$] even if this pathological problem exists.

3. Diagnostics and robustness of the method

The observed radial velocities can be written

$$\mathbf{V}'_r = X\boldsymbol{\theta}_p + \boldsymbol{\varepsilon}, \tag{3.1}$$

where $\boldsymbol{\varepsilon}$ is the observational error and $\mathbf{X}$ and $\boldsymbol{\theta}_p$ are defined as in (2.4). In this case, the estimated vector of parameters corresponding to the minimum of (2.6) is

$$\hat{\boldsymbol{\theta}}_p = (\mathbf{X}^{\mathrm{T}}\mathbf{C}_r^{-1}\mathbf{X})^{-1}\mathbf{X}^{\mathrm{T}}\mathbf{C}_r^{-1}\mathbf{V}'_r, \tag{3.2}$$

where $\mathbf{X}$ is the linearization of X around $\hat{\boldsymbol{\theta}}_p$ (all the nonlinearities are transferred into operator $\mathbf{X}$, removing all the combinations between control variables in the vector θ_p). As in Belsley et al. (1980) and B95, we calculate the condition number of the scaled matrix $\mathbf{Z} = \mathbf{C}_r^{-1/2}\mathbf{X}\mathbf{S}^{-1}$, where $\mathbf{S}$ is a diagonal matrix with the square roots of the diagonal elements of $\mathbf{X}^{\mathrm{T}}\mathbf{C}_r^{-1}\mathbf{X}$. A high condition number is an indication of possible colinearities between fitted parameters, meaning poor robustness and a high uncertainty in the fitted parameters.

When the model is linear in the parameters like in B95, the condition number is quickly available from a singular value decomposition (SVD) of the $\mathbf{Z}$ matrix when this method is used to obtain the analysis. Unfortunately, the SVD method cannot be applied to find the minimum of the cost function here and a SVD is reserved for the end of the minimization procedure. The computation cost is about 30 times greater for the SVD of the $\mathbf{Z}$ matrix than it is for the minimization itself. A special effort would then be needed to optimize the SVD computation if the condition number is to be evaluated on a routine basis.

The variance of the estimated parameters is readily available from the diagonal of the covariance matrix $\mathbf{C}_{pp}$ (not to be confused with the observational-error covariance matrix $\mathbf{C}_r$, which is the statistical expectation of $\boldsymbol{\varepsilon}\boldsymbol{\varepsilon}^{\mathrm{T}}$; see also B95)

$$\mathbf{C}_{pp} = (\mathbf{X}^{\mathrm{T}}\mathbf{C}_r^{-1}\mathbf{X})^{-1}\frac{\boldsymbol{\varepsilon}^{\mathrm{T}}\boldsymbol{\varepsilon}}{N - p}, \tag{3.3}$$

where N is the number of observations and p the number of parameters to retrieve.

For the experiments in this section, we use synthetic observations extracted from a true linear wind and measurements are the radial velocities in cylindrical coordinates. We thus neglect the elevation angles here. We assume that the full volume is collected instantaneously by the virtual radar for each time level. Details of the linear wind field at $t = t_o$ at four vertical levels are depicted in Fig. 1. The profile of vertical motion is positive, parabolic, and null at the bottom and top of the domain. The vorticity also has a parabolic vertical

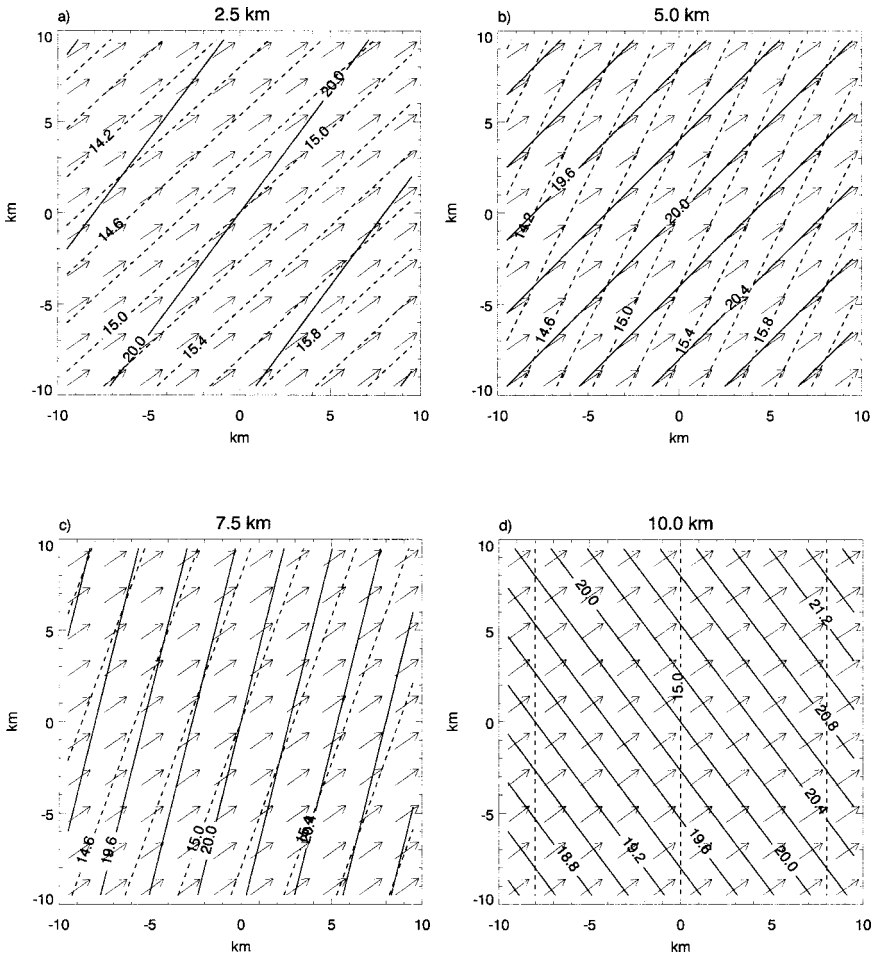

FIG. 1. Linear wind used in section 3. Full lines are isolines of the u component and dashed lines of the v component of the horizontal wind field. Contours are drawn each 0.2 m s^{-1}. Arrows indicate the full horizontal wind vectors.

profile with a positive maximum in the middle of the atmosphere. The shearing and stretching deformations have positive constant values throughout the vertical domain. The system is moving at 9.43 m s^{-1}. The domain size is 20 km $\times$ 20 km^2 with 1-km resolution. Normally distributed random noise of zero mean and a standard deviation of 1 m s^{-1} is added to the radial velocities. The observational-error covariance $\mathbf{C}_r$ is thus simply the identity matrix. When condition numbers or standard deviations of parameters are estimated in this section, no minimization is performed but the correct solution is used for the calculation of the matrix $\mathbf{X}$ and the expression (3.3). All the experiments in this section are performed without any smoothness constraint.

a. Sensitivity to the number of vertical and time levels

Figure 2 shows the standard deviation of the estimated vorticity as function of the number of vertical levels, for assimilation periods of 5 min (two time frames) and 20 min (five time frames). It appears that two vertical levels are sufficient, although this does not guarantee a unique solution. Adding more levels does not significantly decrease the uncertainty in the estimation of vorticity in this case. It is preferable to increase the assimilation period to have a better estimate of vorticity and other parameters in general.

b. Sensitivity to data coverage

We turn now to the evaluation of the method's robustness when data are missing in an azimuth sector of the domain. The experiment is similar to the one in B95 except that we use multiple time levels. This causes the observed azimuth sector to move, as illustrated in Fig. 3. For this end, we use a four-vertical level model (the same as those shown in Fig. 1) with the same flow structure as for the previous experiment. In Fig. 4, the condition number is plotted as a function of increasing sector gap for various assimilation periods. Zero-minute period (solid line) corresponds to a variant of the tra-

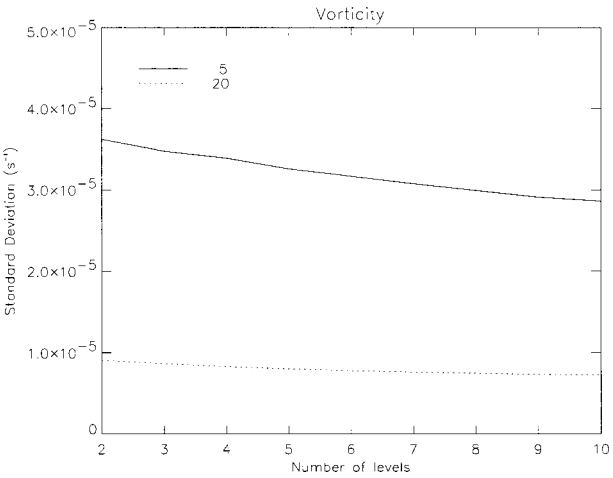

FIG. 2. Standard deviation of estimated vorticity of the highest level when a different number of levels are included in the model, for assimilation periods of 5 and 20 min. The amplitude of true vorticity is 10^{-4} s^{-1}.

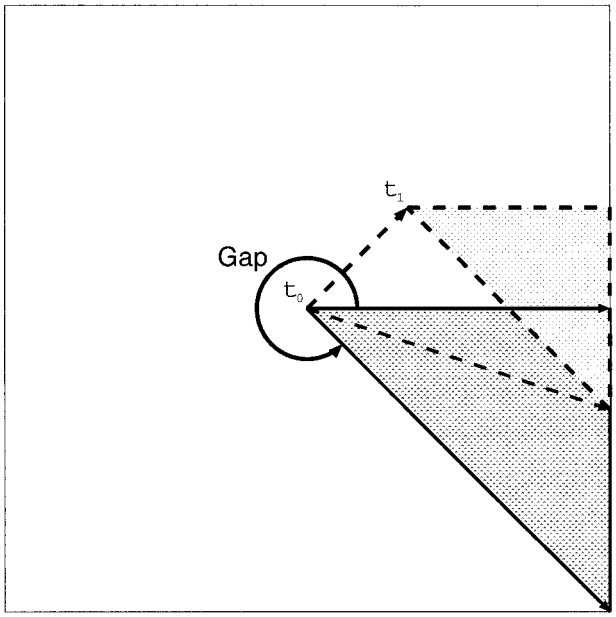

FIG. 3. Schematic representation of the experiment conducted to show the condition number as a function of increasing gap width and assimilation time window. The radar is located in the center of the domain and the storm is moving in the NE direction. The data are in the dotted region. At t_1, the radar measures different components of the wind field than at the initial time t_o.

ditional VVP method (i.e., without analysis of the moving frame and the vorticity). This curve is similar to the one in Fig. 1 of B95. The condition number is relatively constant for a sector gap less than 180°, and increases with increasing assimilation period except for a sector gap greater than 280°. The condition number reaches the critical value of 9–12, suggested by B95 at an assimilation period of 30 min for small sector gaps. Note the better conditioning (lower condition number) for a sector gap greater than 300° for increasing assimilation period.

c. Sensitivity to the system direction displacement

It is noteworthy that the condition number is only a function of observation locations for VVP and not of actual values of the velocity field as is the case for the model (2.2). Indeed, the condition number is sensitive to the moving frame direction displacement, as depicted in Fig. 5. The pairs of parallel moving frame directions (NE, SW; NW, SE) have almost the same condition number for the no gap case. However, all four curves exhibit their own behavior as the gap size is increased. We found that the behavior of the condition number is much more complex with the method proposed here than for VVP. For a given direction displacement, the condition number can be lower for greater sector gap than for full coverage (e.g., SE direction). However, the curves seen in Fig. 5 are representative of the results obtained with other moving frame directions (not shown).

The condition number does not show improvement in robustness of the method in comparison with traditional VVP, except for very large gap size in certain circumstances. However, there is a clear reduction in the uncertainty of the estimated divergence with increasing assimilation period for every sector gap, as shown in Fig. 6. In particular, including several time levels in the analysis permits a greater sector gap before 100% error is reached in the divergence estimation. Similar comments apply for all other parameters, although the moving frame (u', v') and vorticity are not available with traditional VVP.

d. Sensitivity to domain size

When the true wind field is linear and the azimuthal coverage is complete, the condition number equals unity independent of domain radius in the VVP analysis. However, the covariance matrix [Eq. (3.3)] is a measure of the distribution of observations in space and thus is sensitive to the horizontal size of the domain. Clearly, the variance of estimated divergence decreases with increasing domain size, as shown in Fig. 7. All other estimated parameters exhibit the same behavior.

In this section, the linear wind model without the smoothness constraint was tested in an idealized context where the true wind field respects the assumptions of the simplified model. In actual airflows, the assumption of linearity may not be satisfied. This represents model errors that generally lead to biases in the estimated parameters of the model. This effect is well known in regression analysis (Draper and Smith 1981) and has also been studied in the context of radar data assimilation (Caya and Zawadzki 1992; B95). In fact, B95 showed that model error is the most restrictive element for the linear wind analysis. In the next section, syn-

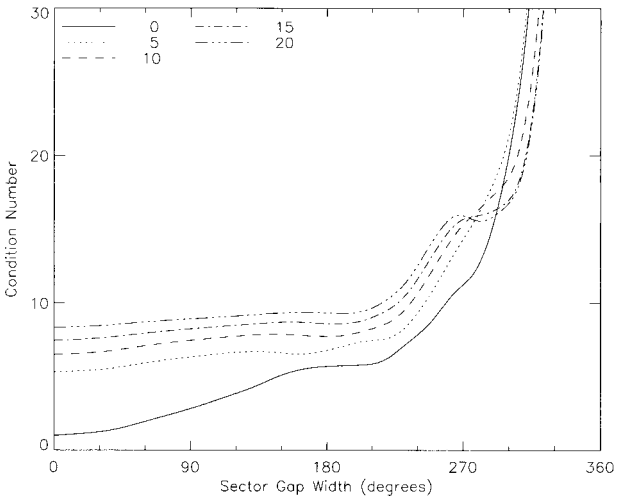

FIG. 4. Condition number as function of increasing sector gap for various assimilation periods (min). Zero-minute period (solid line) corresponds to a VVP analysis. A four-level model is used for this experiment.

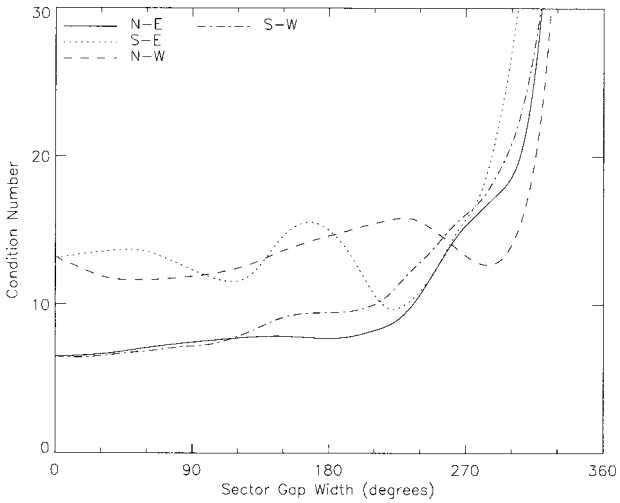

FIG. 5. Condition number as function of increasing sector gap with a 10-min assimilation period and a four-level model. Each line in the legend corresponds to different direction of propagation.

thetic data from a numerical model simulation of convection are presented and will be used to test the sensitivity of the method to model errors.

4. Experiments with model-simulated observations

The synthetic data are generated from the Mesoscale Compressible Community (MC^2) atmospheric model (Laprise et al. 1997). The version of the MC^2 model used to generate the simulated data includes 25 vertical levels with a rigid lid at 25 km. A sponge layer is applied above 15 km. MC^2 is a one-way nested limited-area model. The model simulates a typical convective band that moved over the Montreal region on 16 July 1998. This particular simulation was initiated with a real atmospheric analysis but was not intended to match high-resolution radar observations. In particular, the intensity of the convective activity was larger than what was observed above Montreal during summer storm events. The final high-resolution simulation was realistic but the finescale details do not match the observations. For the first run with a coarse mesh (20 km), the model is initialized with the Canadian Meteorological Centre (CMC) analysis at 1200 UTC on 16 July 1998. The model is integrated over a period of 14 h. The simulation is cascaded down to 10-, 3-, and finally 1-km resolution where the convection is explicit in the model. The 1-km resolution simulation is initiated at 2200 UTC and stopped at 2325 UTC. The resulting 85-min, 1-km resolution simulation with 140×140 horizontal grid points is used as a test bed for the proposed linear wind analysis. Figure 8 depicts the circulation and the reflectivity at a height of 1250 m after 25, 55, and 85 min in the high-resolution simulation. We assume a Marshall and Palmer (1948) raindrop size distribution to compute the reflectivity from the model water content. The band is oriented SW–NE and propagates to the east. At low levels, winds are from the northwest behind the system and from the southwest ahead of the system.

Perfect measurements of single-Doppler velocities are generated directly from the model outputs on a Cartesian grid, with the same terminal velocity as the one used to calculate the radial velocities from the linear wind model. Thus, the choice of the terminal velocity should not affect the results. A normally distributed random noise of zero mean and standard deviation of 1 m s^{-1} is added to the synthetic measurements. Thus, as before the matrix of observational-error covariances $\mathbf{C}_r$ becomes the identity matrix. We also assume that the full volume is collected instantaneously by the virtual radar for each time level.

No synthetic data are available at the initialization time because the precipitation was not initialized. A spinup period is also associated with small-scale adjustment at the beginning of the simulation. For these reasons, only the last hour of simulation ($25 \rightarrow 85$ min) will be considered here. A subdomain of 60 km $\times$ 60 km with 20 vertical levels equally spaced at 500 m is extracted to avoid boundary effects and will be used throughout the study. The data coverage is defined as the grid points whose reflectivity is greater than 15 dBZ. In the 60 km $\times$ 60 km grid, data coverage is about 60% after 25 min in the simulation, reaches a maximum of around 80% at 50–55 min, and then decreases to 55% at 85 min because the system is moving out of the analysis domain.

The linear wind hypothesis is likely to be invalid in convective areas. To avoid contamination of the analysis by convection, only observations where the reflectivity is less than 40 dBZ are used in the retrieval, following B95. After applying this upper reflectivity threshold, the

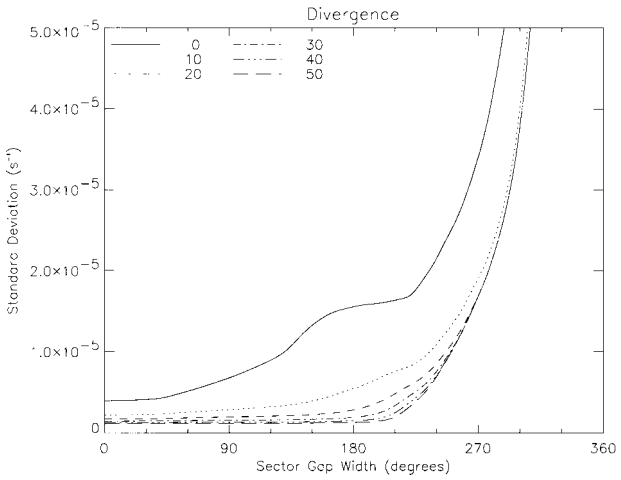

FIG. 6. Standard deviation of estimated divergence of the highest model level as a function of increasing sector gap for various assimilation periods. The amplitude of true divergence is 5×10^{-5} s^{-1}.

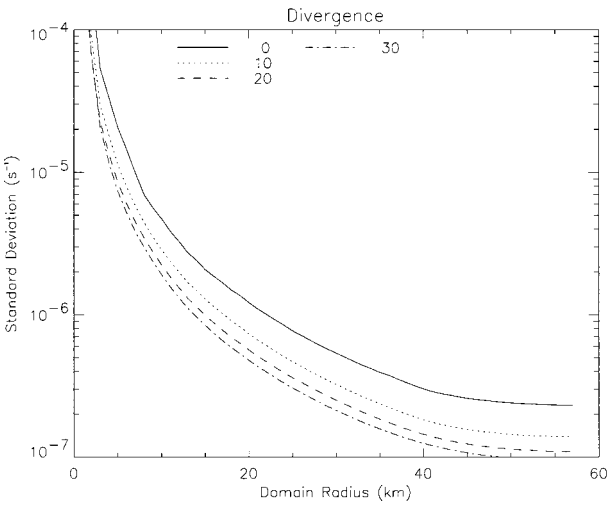

FIG. 7. Standard deviation of estimated divergence of the highest model level as function of increasing domain radius for various assimilation periods. The amplitude of true divergence is 5×10^{-5} s^{-1}.

total data coverage actually used for the linear wind analysis drops from 70% to 41%.

a. Control experiment

In the first experiment, the behavior of the method is investigated in a realistic context. The complex evolution of the nonlinear wind field presented in section 4 is assimilated every 5 min for 1 h. The condition number is 28 for this experiment. The retrieved parameters are compared with the horizontal domain average over the entire assimilation period of the control (Fig. 9). The mean vertical motion is well retrieved except at the top of the domain, where the imposed boundary condition does not correspond exactly to that of the control run. This also affects the divergence profile near the top. The shape of the vorticity profile is generally the same as in the control field. However, the analysis tends to overestimate the amplitude. The stretching and shearing (not shown) deformation are also reasonably well retrieved.

b. Effect of nonlinearity in the wind field

In the second experiment presented here, we test the effect of nonlinearity when the moving frame velocity is specified. For this purpose, the state of the control run at 55 min is advected at a constant speed of (13.3, 3.3) m s^{-1} for 30 min backward in time and 30 min forward in time for a total of 1 h for the assimilation. The linear wind analysis is then performed on that series and a condition number of 21 is obtained. The retrieved moving frame velocity obtained by minimizing Eq. (2.6) is (11.0, 3.4) m s^{-1}, showing that it can be satisfactorily retrieved in the presence of a nonlinear wind field. To evaluate the quality of the other estimated parameters, Fig. 10 compares the analysis with the horizontal time averages of the control. Results are similar to the first experiment (a). It can be concluded that departure from linearity in the wind field is the most important source of retrieval error.

The vorticity can be retrieved because the system is actually scanned from different viewing angles. Viewing angles depend in turn on moving-frame velocity, assimilation period, and position of the scanning radar with respect to the analysis domain. The sensitivity of the retrieval to these three aspects is examined in the following sections.

c. Sensitivity of the moving-frame velocity

Here we show that the translation velocity (u', v') obtained from the motion of the reflectivity pattern does not permit an optimal estimate of radial velocities with the moving linear wind. In Fig. 11, contours of minimized cost function are plotted for different combinations of (u', v'). For each pair of (u', v'), the cost function [Eq. (2.6)] is minimized with the moving-frame velocity held constant. Each minimization is initiated from the previous solution, and moving-frame components are incremented in order to span their entire respective range of values. The minimum is around (15.2, 2.2) m s^{-1}, which is substantially different from the estimation by translation of the reflectivity pattern (10.5, 7.3) m s^{-1}, obtained by minimizing [Eq. (2.9)]. Statistics of the analyzed fitted parameters reveal that the standard deviation of $u_o(z)$ and $v_o(z)$ (not shown) are less than 1 m s^{-1} at all levels when the moving-frame components are varied in the range indicated by Fig. 11, while the sensitivity of the vertical motion is less than 0.022 m s^{-1} (not shown). Figure 12 shows the standard deviation of three retrieved parameters computed with moving-frame components included within the domain depicted

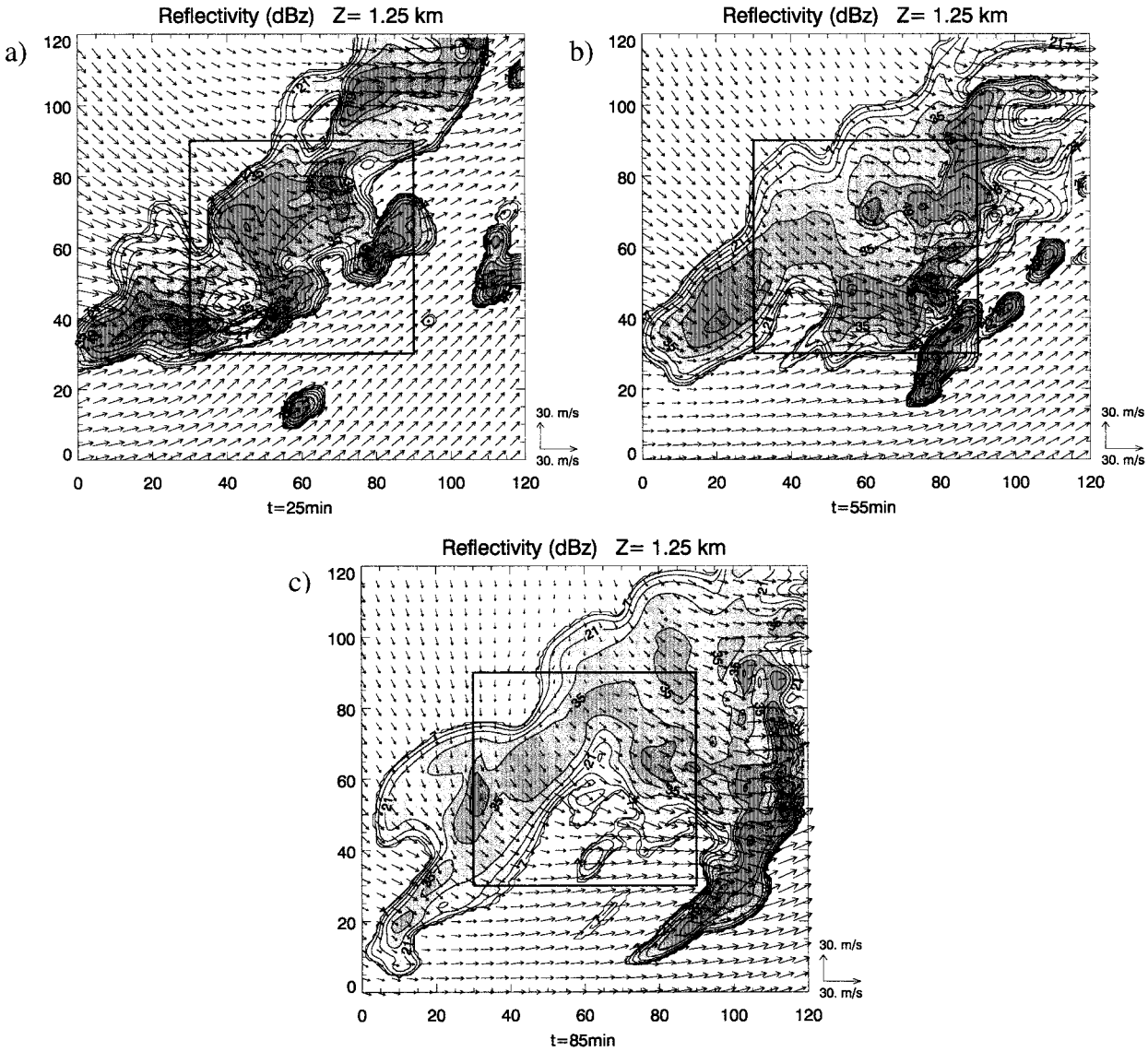

FIG. 8. Horizontal cross sections at height 1250 m and at (a) 25 min, (b) 55 min, and (c) 85 min in the simulation, showing reflectivity (contoured) and winds (arrows). The box indicates the subdomain of 60 km × 60 km used for the experiments.

in Fig. 11. Shearing $\chi(z)$ and stretching $\tau(z)$ deformations have standard deviations of 3×10^{-5} s^{-1} or less, corresponding approximately to a variance of 15% as shown in Fig. 12. The analyzed parameters show little sensitivity to the large range of explored moving-frame velocities. The vorticity $\zeta(z)$, on the other hand, has a much greater sensitivity to the moving-frame velocity.

Moving-frame velocity, when retrieved by minimizing [Eq. (2.9)], seems to correspond to the movement of individual cells within the squall line and does not capture the displacement of the mesoscale system itself. This result is in agreement with the work of Steinacker et al. (1999), who found that the displacement velocity depends on the correlation length used in their reflectivity tracking technique. Here, no preliminary smoothing has been applied to the reflectivity field before the analysis, implying small correlation length. The estimation of the moving-frame velocity from translation of the reflectivity pattern is marginally sensitive to the length of the assimilation period, ranging from (10.1, 6.4) m s^{-1} to (10.5, 7.3) m s^{-1} when the assimilation period varies from 10 to 60 min. However, the analyzed vorticity is quite sensitive to the moving-frame velocity and does not correspond to the best representation of radial velocities (lowest cost function). Thus, we can conclude that it can be hazardous to use the moving frame estimated by translation of the reflectivity pattern for the final velocity displacement of the moving linear wind. Nevertheless, it can be used as a first guess to obtain the optimal moving frame through the minimization of the cost function (2.6). Moreover, smoothing the reflectivity field before analysis can provide a better

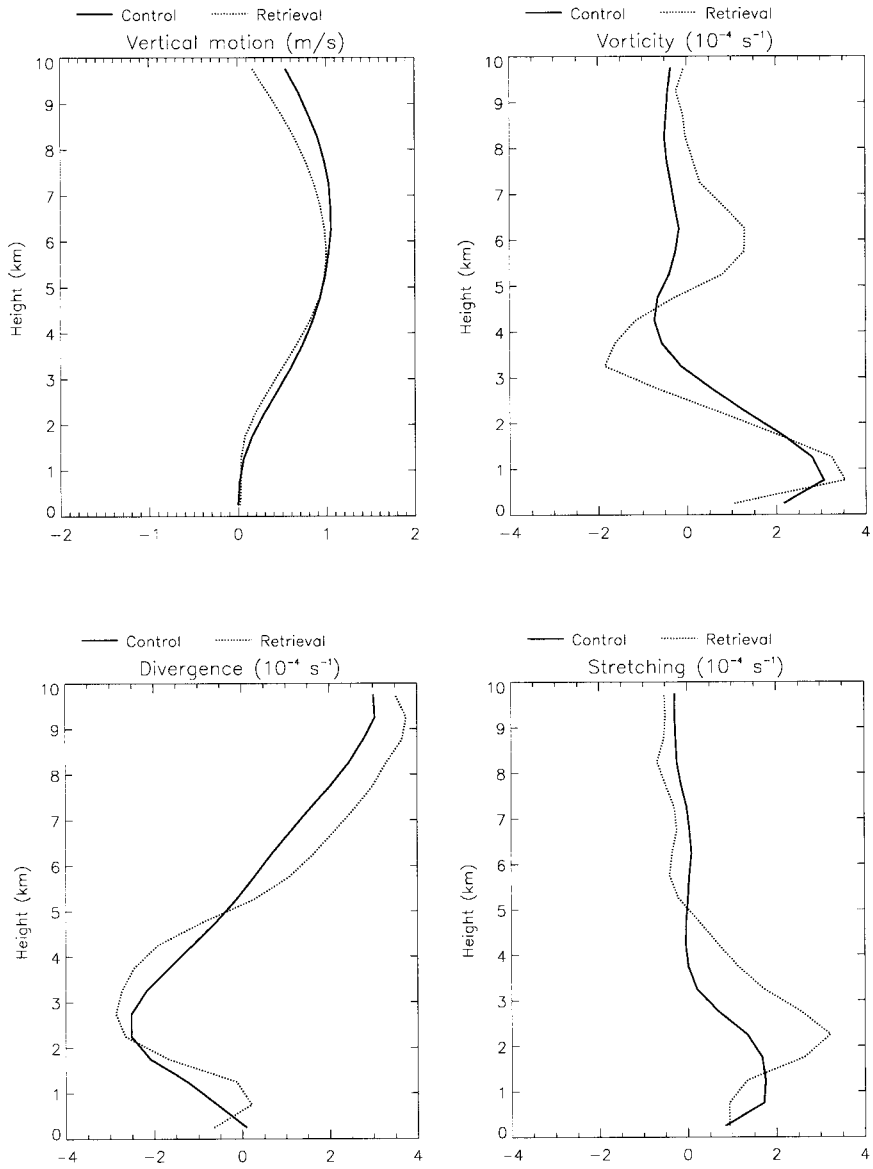

FIG. 9. Comparison between a horizontal time average of the control and retrieved parameters when assimilating nonlinear and nonfrozen flow (experiment of section 4a).

estimate of the mesoscale system displacement, according to Steinacker et al. (1999).

d. Sensitivity to the assimilation period

To assess the sensitivity of the retrieval with respect to the assimilation period, different time windows are considered and the results are evaluated with statistics of the difference between the retrieval and the control in data void regions (where reflectivity is less than 15 dBZ). For the experiments presented here, minimization of the cost function is performed with the moving-frame velocity held constant at (15.2, 2.2) m s^{-1}, which is obtained from the 1-h assimilation period. This simplification is necessary because the three-step minimization procedure described in section 2 falls for short assimilation periods. The verification time is $t = 55$ min, which is the midpoint in the assimilation period.

The effect of increasing the assimilation period is apparent when considering the bias and standard deviation of radial and tangential wind components with respect to the control values. From Table 1, we can see an improvement in tangential wind velocity as more time levels are included in the analysis. However, the bias and standard deviation of the radial component increase with assimilation period for assimilation periods greater than 30 min. This effect is attributed to the fact that the model error also increases with assimilation period.

Table 1 also shows the correlation between retrieved

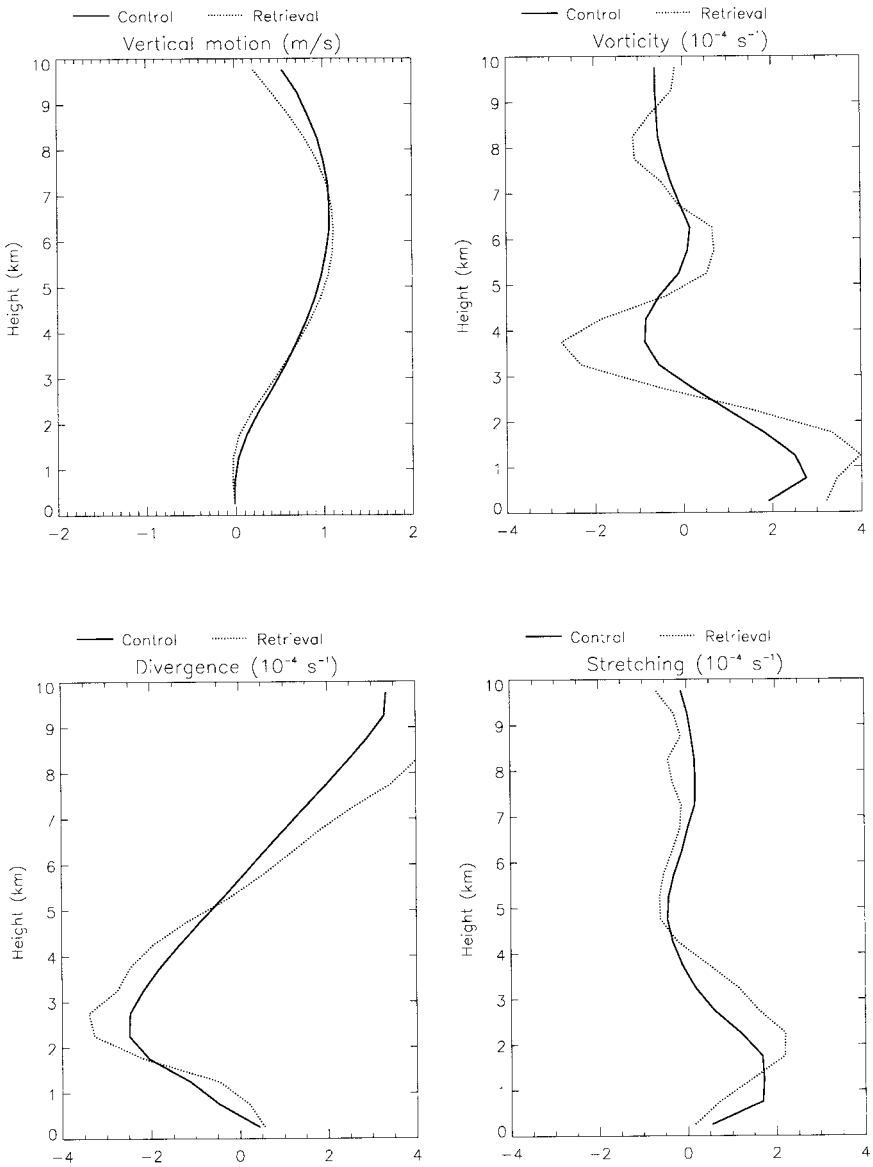

FIG. 10. As in Fig. 9 but for the case where the frozen flow hypothesis is exactly verified (experiment of section 4b).

data and control data for radial and tangential components of the flow. The correlation of radial velocity is high and almost insensitive to the assimilation period. However, the retrieval of the tangential component benefits from a longer assimilation period, up to 1 h for the case studied. It is interesting to note that the correlation for the tangential component is higher than 0.85, even for a short assimilation period of 10 min. In addition, Table 1 shows that the condition number increases with increasing assimilation period (VVP being the lowest), in agreement with the results of section 3. It should be noted that the assimilation period must be large enough (around 40 min for the case studied here) for the method to give better results than VVP, although the latter does not permit the analysis of vorticity.

e. Sensitivity to the radar position

To assess the sensitivity to the radar position, the minimization of cost function is also performed with the moving-frame velocity held constant, which is obtained for the case where the radar is located in the center of the domain. This procedure is again necessary because the minimization fails when the radar is located on the eastern boundary. The assimilation period is 1 h for all experiments.

Again, we evaluate the results by comparing the analysis with the control run in regions of low reflectivity ($<$15 dBZ). As seen in Table 2, the best result is obtained when the scanning radar is located in the center of the domain. Reasonable analyses can also be per-

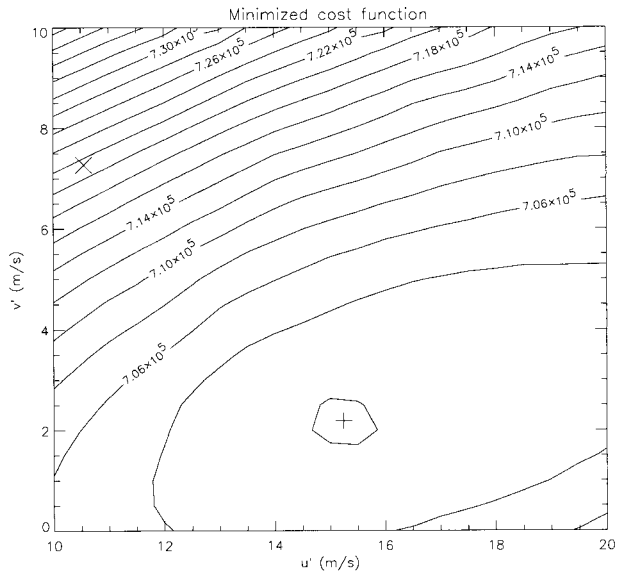

FIG. 11. Minimized cost function as function of (u', v'). Cross $(\times)$ indicates moving-frame velocity estimated by translation of the reflectivity pattern. Plus sign $(+)$ corresponds to moving-frame velocity where the minimized cost function is lowest.

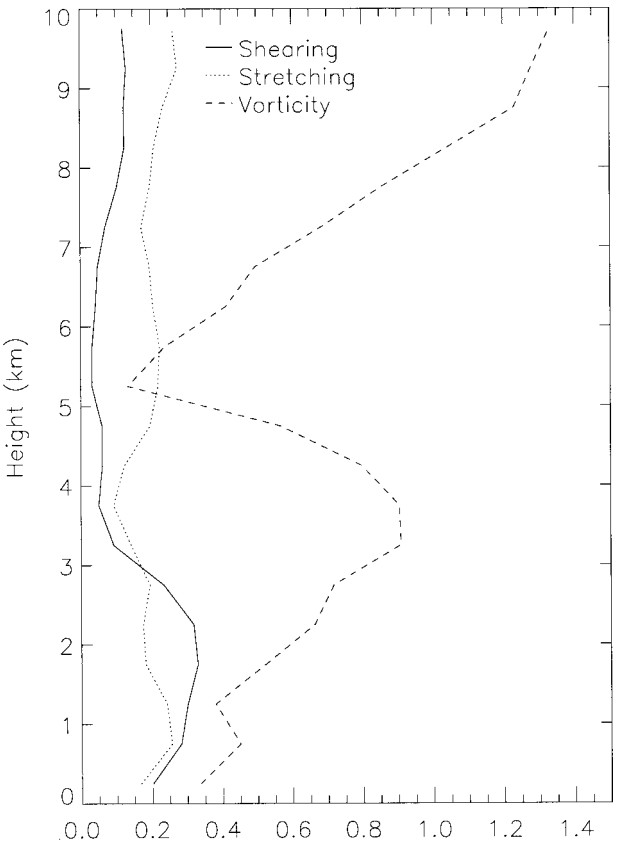

FIG. 12. Sensitivity [expressed in terms of standard deviation $(10^{-4}$ $s^{-1})$] of shearing χ, stretching τ, and vorticity ζ to moving-frame velocity (u', v'). Here (u', v') range as in Fig. 11.

formed when the radar is located in the middle of the southern or the western boundary. The correlation for tangential components decreases for other locations of the radar. This indicates that the radar should be located close to the center of the precipitation area to maximize the difference between viewing angles. This configuration also optimizes the conditioning and the minimization of the cost function.

The condition number is quite sensitive to the position of the radar (Table 2). The two highest values correspond to the two worst cases, and the smaller value to the best case. This confirms that a high condition number is an indicator of difficulty in the minimization. Indeed, the eastern position for the radar corresponds to the highest condition number. The range of values for the condition number in Table 2 can be used to determine the choice of critical value for the quality control.

f. The effect of the smoothness constraint

We now examine the effect of the vertical smoothness constraint on the retrieval. For small values of $\gamma(1–10)$, a marginally better fit to the data is obtained (the global cost function is higher but the term $\boldsymbol{J}_o$ is actually smaller). This is because the smoothness constraint modified the cost function and the minimization algorithm performed better in this situation. The smoothness constraint also permits the model to converge to a solution with short assimilation periods. The vertical profiles of retrieved parameters are smoother as the weight of the smoothing constraint is increased. Figure 13 shows the profile of retrieved parameters for $\gamma = 10\,000$ ($l \approx 10$ km). The greatest change is seen in the vorticity (compare with Fig. 9) because it is the most sensitive parameter. The smoothing diminishes the variability between extremes and brings the retrieval closer to the control.

5. Conclusions

In this paper, we propose a new linear-wind analysis to provide a background wind field for echo-free regions within an analysis domain. By allowing the constant wind field to move at a constant velocity, the vorticity component of the flow can be estimated, allowing us to retrieve a full linear wind field. This is an improvement over the traditional VVP analysis that uses the linear wind approximation only. The method also yields a better estimation of the flow parameters than does VVP. This is because the former takes into account information within a window of time so that the precipitation system can be observed using different viewing angles.

Because the simplified model is actually nonlinear in its parameters, a descent algorithm is used to minimize the cost function associated with the problem. A three-step minimization procedure is adopted to efficiently converge toward the solution. The first step consists of

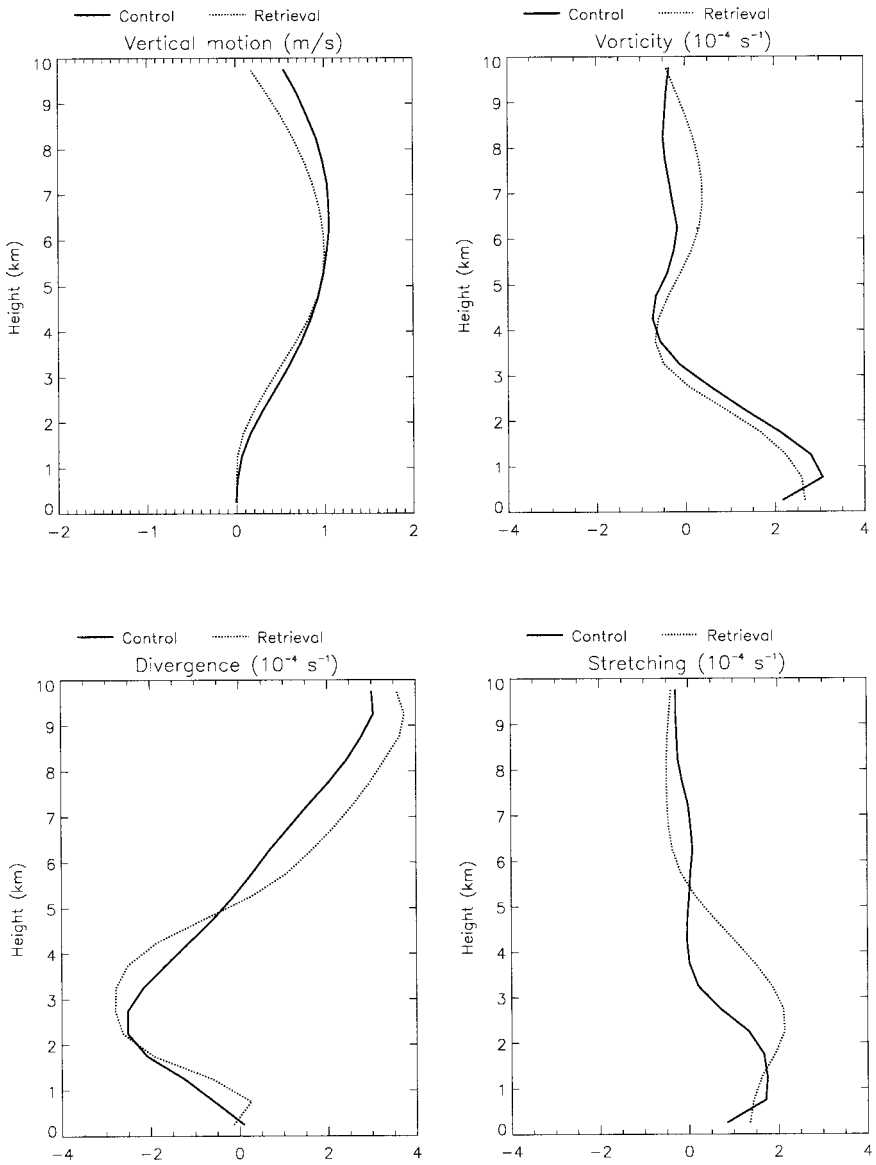

FIG. 13. As in Fig. 9 but for the case with the smoothing constraint.

adjusting the parameters that we find in the traditional VVP analysis, which are the least sensitive. Then, the moving-frame velocity is adjusted while the cost function is further minimized. Finally, the vorticity, which is the most sensitive parameter, is adjusted while the cost function converges to the solution.

The domain of applicability is explored by varying the number of vertical levels and the assimilation period. It is shown that a minimum of three levels is required to avoid multiple solutions, although more levels are preferable. The standard deviation of estimated parameters decreases as the assimilation period increases. For short assimilation periods, the minimization of Eq. (2.6) could fail, although adding a vertical smoothness constraint can help in this case. It is not clear at this point whether this is a problem of multiple local minima or conditioning in the cost function. For longer assimilation periods of up to 1 h, the model error becomes more important but minimization problems are no longer observed with the radar in the middle of the analysis domain.

Following B95, the condition number of the problem is used to diagnose colinearities between retrieved parameters in the method proposed in this paper. A high condition number indicates potential colinearities between retrieved parameters, resulting in poor robustness and high uncertainty in the fitted parameters. The problem is to define a critical value over which spurious analysis can be expected. For our method, serious problems appear only for condition number greater than 30, which is actually the value suggested by Belsley et al. (1980), as opposed to 9–12 for the VVP method studied by B95.

The method is tested with a model-simulated passage of a convective line to assess the impact of the inherent simplifications in the linear wind model. Recall here that the two assumptions in the simplified wind model are the horizontal linearity and that the wind field is moving at a constant velocity. The experiments showed that the nonlinearities in the true wind fields do not prevent the retrieval of the moving-frame velocity. We also argue that the most important source of retrieval errors is the nonlinearities in the true wind fields. However, the scanning characteristics of the radar were not taken into account in this study. We think that this aspect may influence the results presented here and more experiments should be performed to clarify this point.

The possibility of using translation of the reflectivity pattern to estimate the moving frame was studied because removing the moving frame from the control variables (estimated parameters) avoids products between control variables in the cost function. Unfortunately, the moving frame estimated by translation of the reflectivity pattern [Eq. (2.9)] differs from the one that minimizes the cost function [Eq. (2.6)] for the case study. Because the sensitivity of the estimated vorticity to the moving-frame velocity is large, we do not recommand that the moving frame be estimated by translation of the reflectivity pattern. However, this estimate can be used as a first guess in the minimization.

The position of the radar in the analysis domain has a great impact upon the retrieval. The best analysis is obtained when the radar is completely surrounded by precipitation. This position corresponds also to the smallest condition number and best convergence property of the cost function. These results also indicate that the best situations occur when precipitating systems pass just over or close to the scanning radar, guaranteeing a large range of viewing angles.

Additional constraints can be imposed on the wind field to compensate for the lack of information and better conditioning of the problem. They also reduce the effective number of control variables and are generally beneficial in a variational analysis method. Sometimes, it can result in a better fit to the data because it permits better convergence to the solution. The additional constraints also modify the cost function and can mitigate the problem of multiple local minima. The smoothness constraint has proven useful and sometimes necessary in a number of studies and ours is no exception. However, further work is required to set the appropriate weight on the smoothness constraint for real-data analysis. The observational-error statistics are reduced to their simplest expression in this paper and the method would also benefit from further research in the development of a correlation model for the observational-error covariance matrix.

The anelastic vorticity equation can be applied at the convective scale, and this is particularly interesting in single-Doppler retrieval because it depends only on the wind. A few sensitivity tests (not shown) were performed with a vorticity equation applied as a strong constraint to the linear wind. Unfortunately, this constraint leads to additional products among the control variables in the cost function, harming the performance of the minimization. Moreover, a closure term in the vorticity equation for the linear wind would be required. Indeed, the mean vorticity and vertical motion in the model simulation indicate that the closure term is important in this case, especially at the bottom of the domain. In addition, the minimization did not converge to an acceptable solution unless a sufficiently good first guess was used. We therefore discarded this constraint.

The method proposed here will work if a linear wind field defined in a moving frame can approximate the actual environmental flow. It may fail for rapidly developing systems.

The work described here is an integral part of an effort to test the ability of a 4D-VAR method combining a cloud-resolving model with bistatic Doppler radar data for nowcasting purposes. The numerical model is used as a weak constraint and the derived dynamic and thermodynamic fields are used to initialize a stand-alone limited-area numerical model with open lateral boundaries (Montmerle et al. 2001). The 3D environmental wind field proposed here is used to mainly fill data voids. Sensitivity tests indicate that this environmental field has a nonnegligible effect on the initialization and the wind field in radar echo free regions must be made as compatible as possible with the flow within the convective cells.

Acknowledgments. The authors are grateful to Werner Wintels and Rick Danielson, who carefully revised the manuscript. We also thank the three anonymous reviewers who raised many questions that permitted further clarification of the text.

REFERENCES

Belsley, D. A., E. Kuh, and R. E. Welsh, 1980: *Regression Diagnostics: Identifying Influential Data and Sources of Collinearity.* John Wiley and Sons, 292 pp.

Bluestein, H. B., S. D. Hrebenach, and C.-F. Chang, 1994: Synthetic dual-Doppler analysis of mesoscale convective systems. *Mon. Wea. Rev.,* **122,** 2105–2124.

Boccippio, D. J., 1995: A diagnostic analysis of the VVP single-Doppler retrieval technique. *J. Atmos. Oceanic Technol.,* **12,** 230–248.

Browning, K. A., and R. Wexler, 1968: The determination of kinematic properties of a wind field using Doppler radar. *J. Appl. Meteor.,* **7,** 105–113.

Caya, D., and I. Zawadzki, 1992: VAD analysis of nonlinear wind fields. *J. Atmos. Oceanic Technol.,* **9,** 575–587.

Doviak, R. J., and D. S. Zrnić, 1993: *Doppler Radar and Weather Observations.* Academic Press, 562 pp.

Draper, W. R., and H. Smith, 1981: *Applied Regression Analysis.* John Wiley and Sons, 407 pp.

Gal-Chen, T., 1982: Errors in fixed and moving frame of reference: Applications for conventional and Doppler radar analysis. *J. Atmos. Sci.,* **39,** 2279–2300.

Gilbert, J. C., and C. Lemaréchal, 1989: Some numerical experiments

with variable storage quasi-Newton algorithms. *Math. Programming,* **45,** 407–435.

Kilambi, A., A. Protat, A. Singh, I. Zawadzki, J. Wurman, M. Randall, and C. Burghhart, 1997: A bistatic radar system at McGill University. Preprints, *28th Conf. on Radar Meteorology,* Austin, TX, Amer. Meteor. Soc., 45–46.

Klimowski, B. A., and J. D. Marwitz, 1992: The synthetic dual-Doppler analysis technique. *J. Atmos. Oceanic Technol.,* **9,** 728–745.

Koscielny, A. J., R. J. Doviak, and R. Rabin, 1982: Statistical considerations in the estimation of divergence from single-Doppler radar and application to prestorm boundary-layer observations. *J. Appl. Meteor.,* **21,** 197–210.

Laprise, R., D. Caya, G. Bergeron, and M. Giguere, 1997: The formulation of the André Robert MC^2 (Mesoscale Compressible Community) Model. *Atmos.-Ocean,* **35,** 195–220.

Lemaître, Y., and G. Scialom, 1992: Three-dimensional mesoscale circulation within a convective postfrontal system: Possible role of conditional symmetric instability for triggering convective motions. *Quart. J. Roy. Meteor. Soc.,* **118A,** 71–99.

Lhermitte, R. M., and D. Atlas, 1961: Precipitation motion by pulse Doppler. Preprints, *Ninth Weather Radar Conf*., Kansas City, KS, Amer. Meteor. Soc., 218–223.

Lin, Y., P. S. Ray, and K. W. Johnson, 1993: Initialization of a modeled convective storm using Doppler radar-derived fields. *Mon. Wea. Rev.,* **121,** 2757–2775.

Marshall, J. S., and W. M. K. Palmer, 1948: The distribution of raindrops with size. *J. Meteor.,* **5,** 165–166.

Matejka, T., and R. C. Srivastava, 1991: An improved version of the extended VAD analysis of single-Doppler radar data. *J. Atmos. Oceanic Technol.,* **8,** 453–466.

Montmerle, T., and Y. Lemaître, 1998: Three-dimensional variational data analysis to retrieve thermodynamical and dynamical fields from various nested wind measurements. *J. Atmos. Oceanic Technol.,* **15,** 360–379.

——, A. Caya, and I. Zawadzki, 2001: Simulation of a mid-latitude storm initialized with bistatic Doppler radar data. *Mon. Wea. Rev.,* **129,** 1949–1967.

Passarelli, R. E., Jr., 1983: Wind field estimation by single Doppler radar techniques. Preprints, *21st Conf. on Radar Meteorology,* Edmonton, AB, Canada, Amer. Meteor. Soc., 526–529.

Pearce, R. L., Jr., R. A. Brown, and H. G. Camnitz, 1969: Horizontal motion field observations with a single pulse Doppler radar. *J. Atmos. Sci.,* **26,** 1096–1103.

Protat, A., and I. Zawadzki, 1999: A variational method for real-time retrieval of three-dimensional wind field from multiple-Doppler bistatic radar network data. *J. Atmos. Oceanic Technol.,* **16,** 432–449.

——, ——, and A. Caya, 2001: Kinematic and thermodynamic study of a shallow hailstorm sampled by the McGill Bistatic Multiple-Doppler Radar Network. *J. Atmos. Sci.,* **58,** 1222–1248.

Scialom, G., and Y. Lemaître, 1990: A new analysis for the retrieval of three-dimensional mesoscale wind fields from multiple Doppler radar. *J. Atmos. Oceanic Technol.,* **7,** 640–665.

Shapiro, A., S. Ellis, and J. Shaw, 1995: Single-Doppler velocity retrievals with Phoenix II data: Clear air and microburst wind retrievals in the boundary layer. *J. Atmos. Sci.,* **52,** 1265–1287.

Srivastava, R. C., T. J. Matejka, and T. J. Lorello, 1986: Doppler radar study of the trailing anvil region associated with a squall line. *J. Atmos. Sci.,* **43,** 356–377.

Steinacker, R., M. Dorninger, F. Wölfelmaier, and T. Krennert, 1999: Automatic tracking of convective cells and cell complexes from lighting and radar data. *Meteor. Atmos. Phys.,* **72,** 101–110.

Sun, J., and N. A. Crook, 2001: Real-time low-level wind and temperature analysis using WSR-88D data. *Wea. Forecasting,* **16,** 117–132.

Wahba, G., and J. Wendelberger, 1980: Some new mathematical methods for variational objective analysis using splines and cross validation. *Mon. Wea. Rev.,* **108,** 36–57.

Waldteufel, P., and H. Corbin, 1979: On the analysis of single-Doppler radar data. *J. Appl. Meteor.,* **18,** 532–542.

Webster, P. J., and R. Lukas, 1992: TOGA COARE: The Coupled Ocean-Atmosphere Response Experiment. *Bull. Amer. Meteor. Soc.,* **73,** 1377–1416.